

Plasma Polymerization Inside Tubes in Hexamethyldisiloxanes and Ethyne Glow Discharges: Effects of Deposition Atmosphere on Wetting and Ageing in Solvents

Juergen M. Lackner · Martin Wiesinger · Reinhard Kaindl · Wolfgang Waldhauser · Daniel Heim · Paul Hartmann

Received: 7 June 2013 / Accepted: 10 December 2013 / Published online: 9 January 2014
© The Author(s) 2014. This article is published with open access at Springerlink.com

Abstract The coating deposition inside tubes becomes increasingly important for fluidic applications, in which inner surfaces are chemically and mechanically strained by the flowing liquid and by scratching of particles. The developed process for tube coating, presented in this work, is based on the discharge in the precursor gas atmosphere between two mesh electrodes at the ends of the tube. The gas mixture is introduced on one end and pumped through the electrode on the other end. Igniting plasma inside the tube, the tube walls are the barrier to the atmosphere. Especially pulsed DC discharges for plasma polymerization in this alignment lead to good coating results, which is shown in this work focusing on deposition in pure and mixed hexamethyldisiloxane, ethyne, and oxygen atmospheres. Chemical binding, wetting, and ageing are strongly influenced by the choice of the gas mixtures. Sufficient oxygen partial pressure in the deposition atmosphere leads to hydrophilic behavior of the SiO₂-like polymer-like carbon coatings, all other applied atmospheres to generally hydrophobic behavior of pure and Si-doped plasma polymers, respectively.

Keywords Plasma polymerization · Coating of tubes · Hexamethyldisiloxane · Ethyne

Introduction

Plasma polymerization is a unique process for monomer polymerization: While wet chemical polymer formation is based on direct linking of monomers, cross-linking of

J. M. Lackner (✉) · M. Wiesinger · R. Kaindl · W. Waldhauser · P. Hartmann
Research Group Functional Surfaces, Institute for Surface Technologies and Photonics, Joanneum
Research Forschungsges.m.b.H., Leobner Strasse 94, 8712 Niklasdorf, Austria
e-mail: Juergen.lackner@joanneum.at

M. Wiesinger · D. Heim
Faculty of Technical and Environmental Sciences, University of Applied Sciences Upper Austria,
Stelzhamerstrasse 23, 4600 Wels, Austria

fragments of monomer precursors after dissociation in plasma is the basic process in plasma polymerization. Thus, plasma polymerized layers are generally highly cross-linked compared to chemically polymerized polymers. Consequently, these materials are non-soluble, scarcely moisture expanding, highly thermal stable and have higher hardness and scratch resistance but are still elastically deformable. Optical transparency, electrical insulation, semi-permeability, and chemical stability underline their preferred use in scratch resistant layers for optical wave guides and lenses, dielectric layers for condensers, device encapsulation, salt and gas filtering, and corrosion protection [1].

Based on achievable material properties, hexamethyldisiloxane (HMDSO, $[\text{Si}(\text{CH}_3)_2\text{O}]_n$) was applied in this study in a novel deposition setup inside tubes. HMDSO excels by its high vapor pressure at room temperature and its low toxicity compared to other silicon containing precursors (e.g. silanes, tetraethyl orthosilicate) [1]. Such modification of inner surfaces of tubes becomes increasingly important in many applications like fluid transport, being addressed by investigations of the wetting behavior (surface energy) and the stability of the materials in solvents. Although discharges inside tubes are widely applied for lighting since decades, their industrial applications for surface modification and film deposition are rarely found [2–4]. In a previous work [5], we showed the basics of plasma polymerization deposition from hydrocarbon precursors inside tubes with pulsed DC discharges. Most important results of this study focusing on polyacetylene-like coatings were (1) the rather independency of the contact angle from the film thickness for a variety of polymer substrates after homogeneous covering of the surface with smooth films, and (2) the change of the polymerization mode from surface to volume polymerization conditions at low pulse frequencies.

Experimental Details

Film Deposition

The applied coating setup for inner surfaces of tubes is basically comparable to gas discharge lamps. However, the glass tube is replaced by a polycarbonate (PC) polymer tube of 12 mm inner diameter and 50 cm length. For easier characterization of the deposited films, flat PC and (100) silicon substrates were placed inside in the center of this tube, which was changed after each experiment. The setup (Diener Elektronik GmbH, Nagold, Germany), described in detail in [5] (see Fig. 1 too), is afterwards closed on both sides with vacuum flanges, acting as electrodes (cathode and anode). After the evacuation of the tube to 10 Pa base pressure by a fine vacuum pump through the mesh anode, the process gases are delivered to the polymer tube through the mesh cathode. The following gas atmospheres were chosen to obtain different types of film materials. Generally, 60 Pa HMDSO partial pressure is used for deposition of all film types containing silicon atoms, mixed with constantly 80 Pa partial pressure of reactive gases, if necessary. 80 Pa C_2H_2 partial pressure were used for the deposition in pure hydrocarbon atmosphere, being lower limit of the controllability with the available mass flow meters.

- type I: pure HMDSO atmosphere (60 Pa HMDSO),
- type II: HMDSO— O_2 mixtures (60 Pa HMDSO + 80 Pa O_2),
- type III: HMDSO— C_2H_2 mixtures (60 Pa HMDSO + 80 Pa C_2H_2), and,
- type IV: pure C_2H_2 atmosphere (80 Pa C_2H_2).

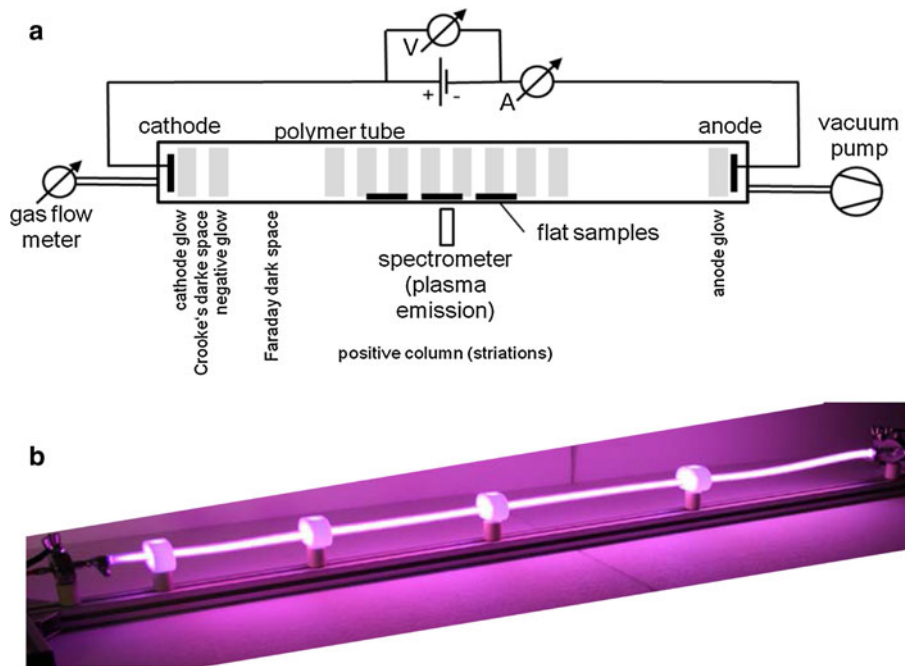


Fig. 1 Applied setup for film deposition in DC discharge inside tubes, whereby the tube wall is the barrier between vacuum and atmosphere: **a** schematics, **b** image taken during ignited plasma [11]

The type II and III films were also deposited at 100 Pa HMDSO partial pressure to show the influence of a higher precursor pressure on the achievable properties.

The plasma modification and coating starts in the pulsed 535 Hz DC discharge between the cathode and the anode with a duty cycle of 15 % (= percentage of active plasma discharge in pulsed plasma). The supplied voltage signal has a rectangular shape with slightly decreasing voltage in the end of the discharge. The control of the gas supply (O_2 , C_2H_2) occurs by gas mass flow meters, the control of liquid HMDSO vaporization by temperature control ($25 \pm 1^\circ C$) and a liquid gas flow meter. Pressure measurement was performed by a Pirani cell and correlated to the applied gas and the precursor vapor types. This pressure was used for the control of the deposition process, allowing a reproducibility of film thickness of $\pm 8\%$. A reproducible modification with nearly constant chemical film composition and contact angles over the tube length is reached in the so called “positive column” of the discharge, which covers $> 90\%$ of the discharge length for 50 cm long tubes [5].

Surface Characterization

The surface quality was inspected by light microscopy. Measurements by stylus profilometry (Veeco DekTak 150) were used for coatings on silicon wafers to obtain film thickness at masked steps. The arithmetic roughness (R_a) was calculated from the measured surface topography. All R_a values were related to the film thickness due to the slight thickness variations at similar deposition durations. The particle density was evaluated by

light microscopy (with $500 \times$ magnification) after cleaning of as-deposited coating surfaces with compressed N_2 .

Contact angle measurements were performed on a home-built system with droplets of de-ionized water ($25^\circ C$) at 55 % relative humidity just after deposition (~ 10 min) and after 90 days storage in ambient air atmosphere (~ 55 % relative humidity, $25^\circ C$). Three droplets of 2 μl volume were used for statistics. All standard deviations were found to be below 3° . The surface energy was calculated using the Owens–Wendt–Rabel–Kaelble and Wu models, applying measured contact angle values from three different test liquids of very different polar and disperse shares of surface tension ($H_2O^{\text{distilled}}$: $\sigma_d = 21.8 \text{ mNm}^{-1}$, $\sigma_p = 51.0 \text{ mNm}^{-1}$; 1,5-pentadiol: $\sigma_d = 27.6 \text{ mNm}^{-1}$, $\sigma_p = 15.7 \text{ mNm}^{-1}$; diiodomethane: $\sigma_d = 50.8 \text{ mNm}^{-1}$, $\sigma_p = 0.0 \text{ mNm}^{-1}$).

Raman investigations of the chemical film composition were obtained by a HORIBA JOBIN–YVON LabRam Raman micro-spectrometer. The samples were measured through an OLYMPUS $100 \times$ objective (N.A. = 0) and excited by the 532 nm emission line of a Nd:YAG laser. The size and power of the laser spot on the surface were approximately 1 μm and 0.01 mW, respectively. The spectral resolution, determined by measuring the Rayleigh line, was about 5 cm^{-1} . The dispersed light was collected by a $1,024 \times 256$ open electrode CCD detector. The confocal pinhole and the spectrometer entrance slit were set to 1,000 and 100 μm , respectively. All spectra were recorded unpolarized. The accuracy of Raman line shifts, checked by regular measuring a Ne spectral calibration lamp, was in the order of 0.5 cm^{-1} . All peak fitting with Gauss-Lorentz functions and applying linear background correction was done by the Labspec 5 software.

X-ray photoelectron spectroscopy (XPS) was employed to investigate the chemical binding in the films using an Omicron Multiprobe system with a monochromized $AlK\alpha$ (1,486.6 eV) X-ray beam and an EA 125 energy analyzer (Omicron GmbH, Traunstein, Germany; resolution better than 0.3 eV). The analysis was carried out at 4×10^{-9} Pa pressure. The spectrometer was operated in the fixed analyzer transmission mode. The detection sensitivity was approximately 1 m %. An Omicron ISE 10 sputter gun using Ar^+ ions was used for sputtering.

The solvent stability of the thin films was tested in distilled water, physiological salt solution, and ethanol at $22^\circ C$. Samples were stored for 1, 3, 10, and 30 days in the solution and changes of the surface with the focus on delamination and film fracture after polymer swelling were investigated by light and scanning electron microscopy.

Results and Discussion

Chemical Composition

During the polymerization of hydrocarbon based gases in plasma, various steps of ionization, radical formation, dissociation and electronic excitation are triggered by inelastic collisions of energized electrons. This results in fragmentation of gas molecules (reactive gases, polymerize-able gases and vapors) [1], leading in the case of HMDSO precursor to oxidized fragments (SiO , SiO_x , $SiO_xC_yH_z$, etc.) and hydrocarbons (CH_x). Preferably, Si–C and C–H bonds are broken in the HMDSO molecule, since the binding energies of Si–C (4.5 eV) and C–H (3.6 eV) are lower than the binding energy of Si–O (8.3 eV) [6–11]. While volatile species like COH_2 , CO_2H_2 , CO, CO_2 , and H_2O are pumped off, fragments as well as simultaneously formed polymerize-able hydrocarbons (CH_4 , C_2H_2) are able to

react on the substrate surface. Ion bombardment and etching, surface diffusion, and carbon etching by oxygen atoms are steps during bond formation and film growth.

In the case of the applied deposition process on the inner sides of tubes, these processes lead in dependency of the gas mixture to very different chemical compositions, as found in XPS investigations: In Table 1, the peak positions of C1 s, O1 s, and Si2p as well as the determined chemical composition (C, O, Si contents) excluding the not detectable H content are given for representative films (deposited at 80 Pa O₂ or C₂H₂ process gas flow) of the investigated three groups of silicon containing coatings (types I–III). Type IV films, deposited in pure C₂H₂ atmosphere and containing only C and O, were not investigated by XPS. A quite stoichiometric ratio of Si:O = 1:2 is clearly evident for the type II film due to oxidation with mixed oxygen. The type I film, deposited in pure HMDSO, contains > 50 % more oxygen and less carbon atoms than the initial HMDSO precursor molecule (Si:O = 1:0.5, Si:C = 1:3). Nevertheless, such high oxygen excess is common for silicone-like plasma polymers [12]. Type III films, deposited in C₂H₂ containing HMDSO plasma () have high carbon, but low oxygen and silicon content. No significant change is evident, if measuring XPS spectra, analyzing peak positions, and calculating atom fractions of C, Si and O on the as-deposited surface and after 2 keV Ar⁺ sputtering to about 10–15 nm depth: The comparison of the elemental composition e.g. for a type I film, grown in pure 100 Pa HMDSO atmosphere, gives: as-deposited/sputtered: 60.1/57.4 at.% C, 17.5/15.8 at.% O, 22.5/26.8 at.% Si.

Further insight to the chemical binding is gained by the comparison of the binding energies (Table 1) with the standard binding energies obtained with AlK α XPS equipment [13]: Generally, the binding energies for C1 s, O1 s, and Si2p are lower for the films grown without O₂ as process gas (type I and III films). Analyzing such Si binding (Si2p peak) in Si containing plasma polymers, polydimethylsiloxane (PDMS) and quartz are generally used as reference materials [14–17]: In PDMS, Si is bound to two carbon atoms and two oxygen atoms (SiO₂C₂, D configuration), while in quartz Si is bound to four oxygen atoms (SiO₄, Q configuration). Binding energies in the range of 101.8–102.1 eV are reported for PDMS and 103.4–103.7 eV for quartz. For SiO₃C (T configuration), the binding energy is estimated assuming the influence of adding one O atom to be equal to half of the difference between these two Si2p peak positions [15]. For the case that Si is bound to one O and three C atoms like in the precursor molecule HMDSO (SiOC₃, M configuration), peak positions of 100.7–101.5 eV are reported. Binding energies between 99.8 and 100.8 eV are attributed to a silicon carbide formation. For the C1 s peak, carbide-type binding is found for 280.8–283.0 eV, C–C binding for 284.0–285.0 eV. Higher energies are due to C–O binding. The O1 s peak at lower energies (531.0–532.0 eV) belongs to hydroxides, medium energies (532.5–532.7 eV) to silicone binding, and high energies (532.5–533.3 eV) to quartz binding [13].

A rough estimation of the chemical shift of the XPS data is enabled by relating the measured binding energies to the O1 s peaks, which are around 532.5–533.0 eV for both silicone and quartz: Based on this assumption, the shift is ~4 eV for the film grown in 100 Pa HMDSO (type I), ~3.5 eV for 100 Pa HMDSO + 80 Pa C₂H₂ (type III) ~3 eV for 100 Pa HMDSO + 80 Pa O₂, and ~0 eV for 60 Pa HMDSO + 80 Pa O₂ (type II) Adding these chemical shifts confirms for the type II films SiO₄ quartz binding (Q configuration) based on the Si2p doublet. However, the existing Si2p doublets as double peaks let expect further binding contributions: The Si2p doublet at lower energy and with lower intensity indicates contributions of D to the large content of Q configuration binding.

The type I and III films are rather similar: Corrected C1 s binding energies seems to indicate C–C binding, Si2p doublet energies M configuration binding. Silicone (PDMS)

Table 1 Peak position for C1 s, O1 s, and Si2p peaks as well as elemental composition (except H) of the coatings deposited in HMDSO, HMDSO + O₂, and HMDSO + C₂H₂ atmospheres inside tubes on silicon wafers (XPS measurement on film surface)

	C1 s (eV)	O1 s (eV)	Si2p doublet (eV)	C (at.%)	O (at.%)	Si (at.%) _{ss}
60 Pa HMDSO (type I)	280.6	528.2	97.6, 98.2	60.1	17.5	22.4
				Si:C ratio = 1:2.68, Si:O ratio = 1:0.78		
60 Pa HMDSO + 80 Pa O ₂ (type II)	285.7	533.7	99.0/103.9, 99.6/104.5	6.8	61.4	31.8
				Si:C ratio = 1:0.21	Si:O ratio = 1:1.93	
100 Pa HMDSO + 80 Pa C ₂ H ₂ (type III)	280.9, 282.8	528.5, 529.8	97.4, 98.0	72.2 C–O binding content	20.3	7.46
				Si:C ratio = 1:9.68, Si: O ratio = 1:2.72		

Error limits generally $< \pm 0.2$ eV

binding is rather missing for these films. Additionally, two C1 s peaks, of which one is very high, confirm contributions of a C–O binding for the type III film.

Increasing the HMDSO partial pressure to 100 Pa slightly changes the chemical composition, but does not significantly change the binding energies: In a representative type II film, deposited with additional 80 Pa O₂, the carbon content increases to about 14 % due to less carbon etching by oxygen, while in a type III films, grown in HMDSO and 80 Pa C₂H₂, the silicon content increases to about 10 at.%.

XPS investigation of polymer-like carbon (PLC) films (type IV) without Si content does not give further insight in the chemical binding. Similarly, the sp² and sp³ hybridization of the carbon atoms is also not accessible for all the other film types by XPS. Alternatively, Raman spectroscopy was chosen. Exemplary, Raman spectra for type II, III, and IV coatings are shown in Fig. 2 for film with 80 Pa C₂H₂ and O₂ process gas pressure. Similar to XPS, a variation of O₂ and C₂H₂ gas pressure at similar HMDSO pressure was not found to influence these Raman spectra significantly. The high luminescence background, indicative for high hydrogen contents >20 % [18], was subtracted from all Raman spectra to improve the visibility of peaks. Consequently, a poor signal-to-noise ratio causes relatively large errors in the fitting procedures. Nevertheless, some general features are present in the spectral range of ~ 800 – $2,000$ cm⁻¹, in which all carbons show their dominating features. No carbon related peaks are occurring for the type II coating revealing the absence of carbon related species. The sharp peak at ~ 970 cm⁻¹ is related to the SiO_x, covering the Si substrate. In contrast, all other shown films contain a sufficient amount of carbon atoms for forming the representative carbon peak features: The so called D band (disordered), which is present at $\sim 1,360$ cm⁻¹, occurs for type IV films, the G band (graphite) at $\sim 1,560$ cm⁻¹ (19 and references therein) for type III and IV films. The G and D bands are due to vibrations of sp² sites: The G band has its origin in the bond stretching of all pairs of sp² atoms in rings and chains, and the D band originates from the breathing modes of the sp² carbon rings [20, 21]. Absence of a D-peak in the type III films suggests the dominance of chain groups over rings [19]. The FWHM of the G-peak of more than 240 cm⁻¹ indicates in-plane correlation lengths below 1 nm for type III and IV films.

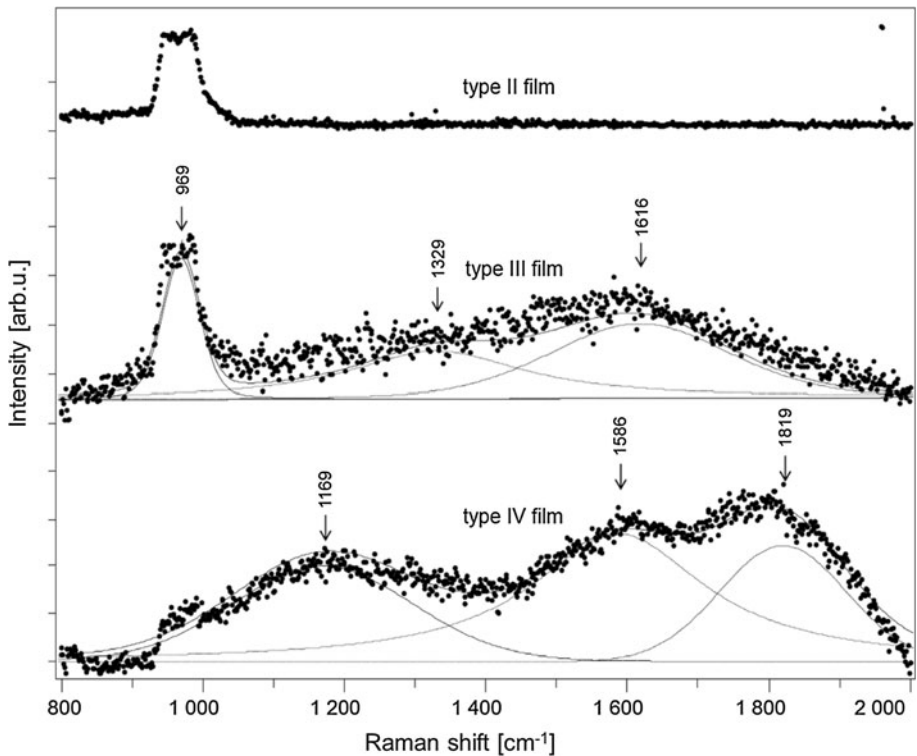


Fig. 2 Raman spectra for the films deposited in 60 Pa HMDSO and 80 Pa O₂ (type II), 60 Pa HMDSO and 80 Pa C₂H₂ (type III), and 80 Pa C₂H₂ (type IV). The *circles* indicate the measured data points, the *stippled* and *dotted curves* represent the Gauss-Lorentz functions and the *solid curves* the sum of the deconvoluted functions

The broad peaks at $\sim 1,200\text{ cm}^{-1}$ for type III films could result from CH compounds, e.g. phenyl ring vibrations of styrene monomers. The bands at $\sim 1,820\text{ cm}^{-1}$ in type III films might be explained by symmetrical and antisymmetrical stretching vibrations of (C = O)₂ in carbocyclic open chain anhydrides [22]. Any linear carbon chains with sp hybridization can be excluded since the indicative “C”-peak at about $2,100\text{ cm}^{-1}$ [23] was not observed.

Such chemical compositions are possible because plasma polymerized films consist of different monomer segments, which are stringed together heterogeneously. This structure is contrary to a “normal”, ordered macromolecular polymer structure. The whole polymerization occurs predominately by radical mechanisms due to the mostly lower dissociation energy compared to the ionization energy of the monomers. UV radiation, which is generated due to the relaxation processes in electronically excited species, assists the polymerization inducing both the cross-linking and the chain cutting [1].

Growth Rate, Roughness and Wetting

The strong variation in chemical compositions due to the variation of the gas mixtures has decisive effects on the film properties, especially on the wetting behavior, while the roughness (related to film thickness) is rather not affected.

Type II films, grown in 60 Pa HMDSO + O₂ mixtures, were found to be highly hydrophilic with contact angles between 10 and 30°, independently of the substrate and film thickness on PC (113°) and glass substrate (48°) after homogeneous surface covering at 15–20 nm (Fig. 3). Lower values are always present for just-deposited type II films, higher values for 90 days aged films under atmospheric conditions. Contrary aging results are found for type I films with hydrophobic properties (deposited in 100 Pa HMDSO + O₂ mixtures): The deposition rates of these films are about 30 % lower than for type I films. This behavior is most probably due to distinct carbon etching by oxygen atoms, visible in the quite stoichiometric chemical composition, as shown above. Interestingly, the HMDSO pressure of 100 Pa increases the deposition rate to the more than the double value and changes the water contact angle to hydrophobic levels (Fig. 3). In contrast, the aging behavior of these films with increasing contact angle is similar to the films, grown in 60 Pa HMDSO. This intermediate behavior of deposition in 100 Pa HMDSO seems to be correlated to the higher carbon content in these films compared to the deposition in 60 Pa HMDSO, being far from the level of type I films. Comparing the surface energy values, the deposition in pure HMDSO results in a polar component σ_s^p of 19.4 mNm⁻¹ and a dispersive component σ_s^d of 1.6 mNm⁻¹ after 90 days on PC substrate ($\sigma_s^p = 33.4$ mNm⁻¹, $\sigma_s^d = 2.2$ mNm⁻¹). The mixing different pressure of oxygen to the deposition atmosphere with 60 Pa HMDSO (type II films) results in $\sigma_s^p = 45.0$ – 46.2 mNm⁻¹ and $\sigma_s^d = 2.0$ – 2.1 mNm⁻¹. The intermediate behavior of films grown in 100 Pa HMDSO is correlated to contact angles of $\sigma_s^p = 21.4$ – 23.6 mNm⁻¹ and $\sigma_s^d = 4.5$ – 7.4 mNm⁻¹ in the investigated range of oxygen addition. Such dispersive components of the surface energy are due to Lifshitz-van der Waals forces during the interaction of the liquid with the surface; The polar components originate from polar interactions and Lewis acid–base binding.

These results for the deposition in HMDSO atmospheres with different oxygen content follow the theories for deposition in low pressure glow discharges [6–9]: Carbonated radicals and abstracted methyl radicals are directly deposited and undergo homogeneous oxidation reactions or reactions with hydrocarbons. The fragments may then adsorb on the surface and the carbonated species are oxidized by (atomic) oxygen. At high dilution conditions (high O₂/HMDSO flow ratios, in this work at a partial pressure rate O₂/(HMDSO + O₂) = 0.45–0.5), these heterogeneous oxidation reactions are dominating and responsible for a drastic reduction of the carbon content in the films. Depending on the kinetic energy of the impinging ions, active sites are formed by bond scission. Furthermore, etching of smaller species occurs. The ion bombardment is also responsible for densification and smoothing of the growing film.

In contrast to deposition in O₂ process gas, mixing of C₂H₂ in type III films does not drastically change the film properties of the type I films: Hydrophobic behavior is found independently on the C₂H₂ gas partial pressure both for 60 and 100 Pa HMDSO partial pressure (Fig. 4). A change to hydrophilic properties is missing, which is due lack of etching and oxidation reactions by oxygen atoms (silicon oxide formation). Thus, both HMDSO and C₂H₂ molecules are dissociated in plasma and fragments are polymerized. Similar hydrophobic behavior is found for Si-free type IV films (C₂H₂ fraction = 1). A small influence on the water contact angle was found for the silicon content: Increasing C₂H₂ fraction in the process gas lowers both for 60 and 100 Pa the H₂O contact angle from 105 to 115° in pure HMDSO to 90–95° in pure C₂H₂. 90 days aging generally decreases the contact angle by about 20–25°.

Additionally, the growth rates in HMDSO and C₂H₂ mixtures are on a rather stable level compared to the deposition in pure HMDSO or C₂H₂ atmospheres. Surface energies for deposition in 60 versus 100 Pa HMDSO partial pressure follow the trend found for contact

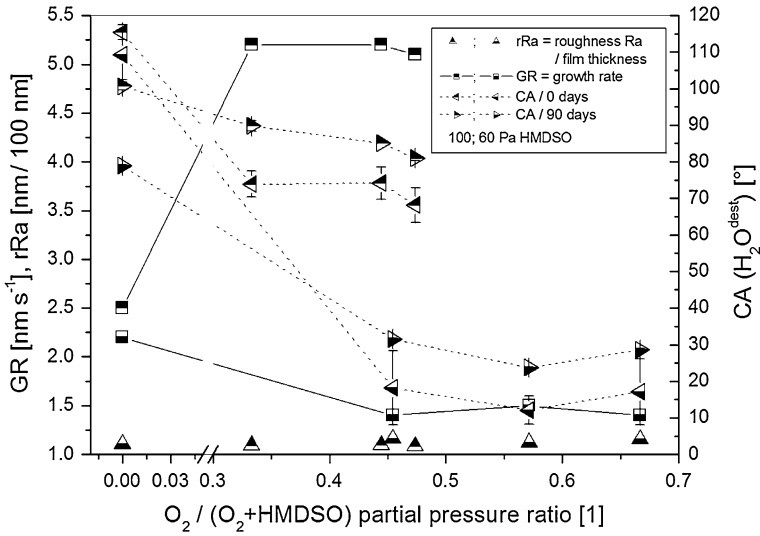


Fig. 3 Dependency of the growth rate (GR), the arithmetic roughness (R_a) related to the film thickness (nm) (“rRa”), and the H_2O^{dest} contact angle (CA) (25 °C, 55 % r.h.), measured after deposition (0 days) and after 90 days aging in ambient atmosphere, on the $O_2/(O_2 + HMDSO)$ partial pressure ratio. The lines connect measured points at different O_2 partial pressures for 60 and 100 Pa HMDSO pressure, respectively. Type I films, deposited in pure HMDSO, are shown at a ratio of 0.0

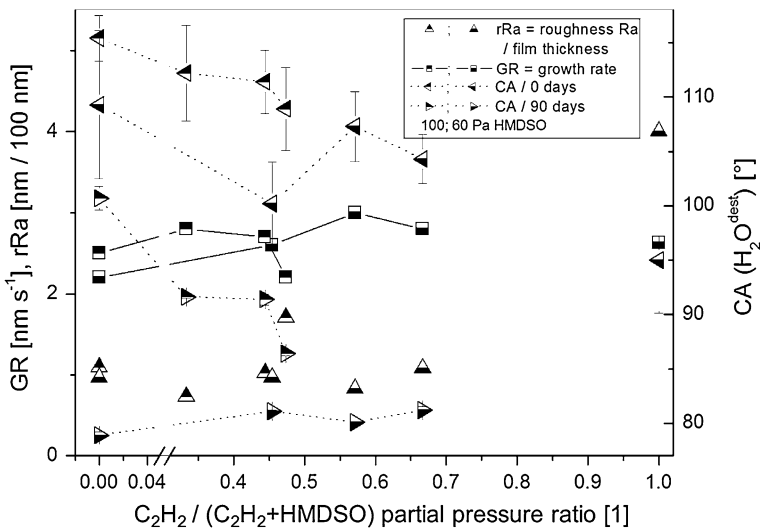


Fig. 4 Dependency of the growth rate (GR), the arithmetic roughness (R_a) related to the film thickness (nm) (“rRa”), and the H_2O^{dest} contact angle (CA) (25 °C, 55 % r.h.), measured after deposition (0 days) and after 90 days aging in ambient atmosphere, on the $C_2H_2/(C_2H_2 + HMDSO)$ partial pressure ratio. The lines connect measured points at different C_2H_2 partial pressure for 60 and 100 Pa HMDSO pressure, respectively. The type I films, deposited in pure HMDSO, are shown at a ratio of 0.0, the type IV films from deposition in pure C_2H_2 at a ratio of 1.0

angles: They decrease with increased HMDSO flow from $\sigma_s^p = 33.5\text{--}35.7 \text{ mNm}^{-1}$, $\sigma_s^d = 4.2\text{--}4.4 \text{ mNm}^{-1}$ to $\sigma_s^p = 25.3\text{--}29.8 \text{ mNm}^{-1}$, $\sigma_s^d = 2.5\text{--}3.4 \text{ mNm}^{-1}$. A significant different behavior of deposition in HMDSO (+ C₂H₂) and pure C₂H₂ atmosphere is only found in roughness related to the film thickness: It increases by a factor of 2 for film growth in pure C₂H₂. In former investigations [5] this roughening of these type IV films was found to be due to a change from surface polymerization to partly volume polymerization mode, accompanied by the deposition of particles and clusters. A mild roughening is also evident in the type III films: Increasing C₂H₂ flow increases the amount of light microscopically counted large particles on Si wafer surfaces from 1 mm⁻² to about 3–4 mm⁻² for 40 and 80 Pa C₂H₂ mixing, respectively. No such defects are found for type I and II coatings.

Ageing of Coatings in Solvents

To gather effects on the film adhesion by polymer substrate swelling due to soaking of liquids and polymer degradation, all 4 film types on PC substrates were stored in deionized water, physiological salt solution, and ethanol at constant temperature of 22 °C for distinct durations (1, 3, 10, and 3 days). The light and scanning electron microscopy inspection of the surfaces after testing revealed both before and after wiping with paper towels no visible changes (no traces of degradation or delamination) for all aging durations. The type-III coatings (100 Pa HMDSO + 80 Pa C₂H₂) are covered with a network of cracks, which becomes slightly denser at the longer ageing durations. However, even wiping does not lead to delamination. PC degradation was not found in any case.

Conclusions

A coating setup based on a pulsed DC discharge was used for deposition of plasmapolymer films on the inner faces of tubes. HMDSO, O₂ and C₂H₂ were used as precursor and reactive gases, leading to silicon oxide and (silicon containing) polymer-like carbon deposits of very different wetting behavior, while the topography (roughness) of the films was rather not influenced. Silicon oxide like films (with largely SiO₄-type binding) grown in mixtures of HMDSO and sufficient oxygen (partial pressure O₂ : HMDSO > ~ 1:1) are found to be hydrophilic. Too low O₂ partial pressure in the HMDSO-O₂ deposition atmosphere results in hydrophobic behavior similar to polymer-like carbon deposits from pure HMDSO or C₂H₂ as well as from HMDSO and C₂H₂ mixtures. Insufficient oxygen for carbon etching during deposition results in a transition behavior of wetting. In solvents, the coatings behave stable—traces for delamination as well as for PC substrate degradation after 30 days of aging are missing.

Acknowledgments All financial support of this work by the Austrian Federal Ministry of Traffic, Innovation and Technology, the Austrian Industrial Research Promotion Fund (FFG) within the frame of the MNT-ERA.NET program, the Government of Styria, and the European Union in the frame of EFRE is highly acknowledged.

Open Access This article is distributed under the terms of the Creative Commons Attribution License which permits any use, distribution, and reproduction in any medium, provided the original author(s) and the source are credited.

References

1. Biederman H (2004) Plasma polymer films. Imperial College Press, London
2. Karwoski T, Matsuzawa Y (1986) Glow discharge process for producing implantable devices. US Patent 4.632.842
3. Cao L, Ratner BD, Horbett TA (2007) *J Biomed Mater Res A* 81:12–23
4. Biedermann A (1986) Process for the interior coating of electrically non-conducting hollow bodies. EP 0262323
5. Lackner JM, Kahn M, Waldhauser W (2011) *Vacuum* 86:144–150
6. Favia P, d'Agostino R, Fracassi F (1994) *Pure Appl Chem* 66:1373–1380
7. Lamendola R, d'Agostino R, Fracassi F (1997) *Plasmas Polym* 2:147–164
8. Magni D, Deschenaux C, Hollenstein C, Creatore A, Fayet P (2001) *J Phys D* 34:87–94
9. Fracassi F, d'Agostino R, Fanelli F, Fornelli A, Palumbo F (2003) *Plasmas Polym* 8:259–269
10. Goujon M, Belmonte T, Henrion G (2004) *Surf Coat Technol* 188–189:756–761
11. Wang Y, Zhang J, Shen X (2006) *Mater Chem Phys* 96:498–505
12. Balkova R, Zemek J, Cech V, Vanek J, Prikryl R (2003) *Surf Coat Technol* 174–175:1159–1163
13. Moulder JF, Stickie WF, Sobol PE, Bomben KD (2002) *Handbook of x-ray photoelectron spectroscopy*. Perkin-Elmer, Eden Prairie
14. Grüniger A, Bieder A, Sonnenfeld A, von Rudolf Rohr P, Müller U, Hauert R (2006) *Surf Coat Technol* 200:4564–4571
15. Alexander MR, Short RD, Jones FR, Michaeli W, Blomfield CJ (1999) *Appl Surf Sci* 137:179–183
16. O'Hare LA, Hynes A, Alexander MR (2007) *Surf Interf Anal* 39:926–936
17. Roualdes S, Berjoan R, Durand J (2001) *Separ Purif Technol* 25:391–397
18. Casiraghi C, Ferrari AC, Robertson J (2005) *Phys Rev B* 72:085401-1-14
19. Robertson J (2002) *Mater Sci Engin R* 37:129–281
20. Tunistra F, Koenig JL (1970) *J Chem Phys* 53:1126–1130
21. Ferrari AC, Robertson J (2000) *Phys Rev B* 61:14095–14107
22. Nyquist RA (2001) *Interpreting infrared, Raman, and nuclear magnetic resonance spectra*, vol 1. Academic Press, San Diego, p 446
23. Ravagnan L, Sivier F, Lenardi C, Piseri P, Barborini E, Milani P, Casari C, Li Bassi A, Bottani C (2002) *Phys Rev Lett* 89:285506–285509